How to cite: Angew. Chem. Int. Ed. 2024, e202313944
doi.org/10.1002/anie.202313944

DNA Nanotechnology

Design and Thermodynamics Principles to Program the Cooperativity of Molecular Assemblies

*Dominic Lauzon and Alexis Vallée-Bélisle**

Abstract: Most functional nanosystems in living organisms are constructed using multimeric assemblies that provide multiple advantages over their monomeric counterparts such as cooperative or anti-cooperative responses, integration of multiple signals and self-regulation. Inspired by these natural nanosystems, chemists have been synthesizing self-assembled supramolecular systems over the last 50 years with increasing complexity with applications ranging from biosensing, drug delivery, synthetic biology, and system chemistry. Although many advances have been made concerning the design principles of novel molecular architectures and chemistries, little is still known, however, about how to program their dynamic of assembly so that they can assemble at the required concentration and with the right sensitivity. Here, we used synthetic DNA assemblies and double-mutant cycle analysis to explore the thermodynamic basis to program the cooperativity of molecular assemblies. The results presented here exemplify how programmable molecular assemblies can be efficiently built by fusing interacting domains and optimizing their compaction. They may also provide the rational basis for understanding the thermodynamic and mechanistic principles driving the evolution of multimeric biological complexes.

Introduction

Nanomachines in living organisms are at the basis of life,[1] and are inspiring the development of many self-assembled nanotechnologies with numerous applications.[2] The majority of natural biomolecular nanomachines are composed of multiple molecular components that need to self-assemble to trigger specific functions and cellular responses.[3] Molecular assemblies have been shown to provide both structural and functional advantages. These advantages include the creation[4] or stabilization[5] of active sites, as well as the creation of new self-regulated mechanisms through allostery[3a] and/or configurational cooperativity.[6] Inspired by these natural nanomachines, numerous researchers are designing artificial assemblies with similar properties using biomolecules such as proteins,[7] peptides,[8] DNA,[9] RNA,[10] or by using chemically synthesized molecules such as crown ethers,[11] calixarenes,[12] or foldamers.[13] For example, Lim et al. have demonstrated how multi-domain protein receptors can help programming the level of cooperativity of an output response.[7a] Similarly, Ricci et al. have demonstrated how to optimize the input/output response of DNA-based unimolecular pH-dependent switches[9a] and dimeric DNA-based nanodevices.[9b] Stoddard et al. have shown that pH-responsive nanomachines can also be synthesized from synthetic macrocycles.[11b]

Although constructing novel molecular assemblies remains an interesting challenge, programming their dynamics of assembly represents the next challenge to develop efficient artificial biotechnologies. In biosensing and drug delivery, for example, it remains important to have precise control over the transduction of a binding event, or assembly, into a specific output (i.e., detection of an analyte or liberation of drugs). In such nanosystems, the output response is typically programmed to activate at the required concentration and with the right sensitivity. In exploring this effect, Plaxco et al., for example, have applied many nature-inspired strategies to program the "useful dynamic range" of biological recognition elements.[14] Fesik et al. have demonstrated how bidentate ligands can considerably improve the host–guest affinity between a ligand and its specific protein receptor,[15] while Schalley et al. have shown how to program the affinity and cooperativity in divalent crown ether nanosystem.[16] However, even though the programmability potential of self-assembled nanosystems has been previously demonstrated, most of these examples remain focused on the optimization of monomeric entities or dimeric host–guest systems. Since nanosystems involving more than two components have been shown to display various functional advantages over their monomeric or dimeric counterparts[3d] and are becoming increasingly important in the development of future nanotechnologies,[2] a better understanding of how these self-assembled nanosystems can be designed, programmed, and optimized is needed.

One strategy employed by nature and chemists to create new functional assemblies consists of fusing interacting domains to promote their complexation. (Figure 1-I, *left*).[17]

[*] D. Lauzon, Prof. A. Vallée-Bélisle
Laboratory of Biosensors & Nanomachines, Department of Chemistry, Université de Montréal
Montréal, QC, H2V 0B3 (Canada)
E-mail: a.vallee-belisle@umontreal.ca

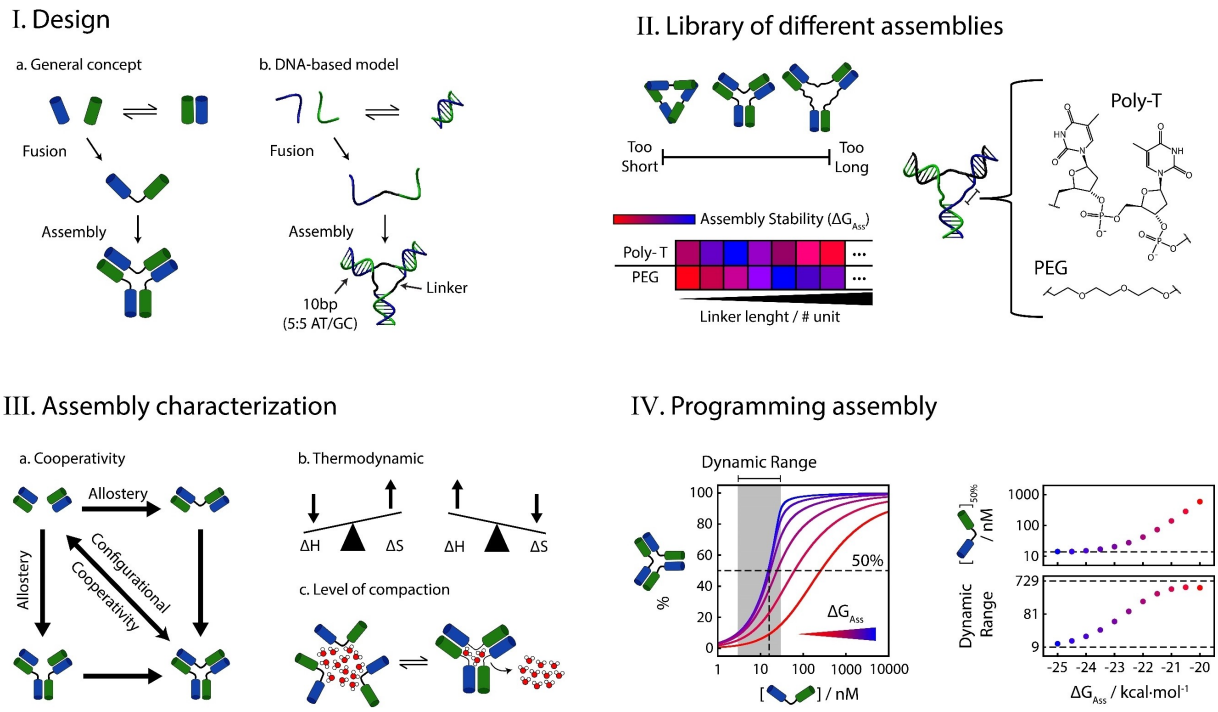

Figure 1. Programming molecular assemblies by connecting interacting domains. I. Design. *Left.* A trimeric assembly can be engineered through the assembly of three components built by linking two interacting domains (blue and green) together using a linker (black). *Right.* Our model system consists of a DNA interacting domains (10 nucleotides) connected via a linker that specifically form a trimeric assembly. Of note, binding domains were specifically designed to favour trimeric assembly over monomers or dimers (see DNA sequences in Supporting Information). II. Library of different assemblies. We prepared a library of trimeric assemblies with different stability (ΔG_{Ass}) by varying the linker connection (e.g., poly-T, PEG, length, ...), with shorter linkers expected to prevent some interaction due to steric hindrance and longer linkers expected to compromise assembly due to higher entropic cost. III. Assembly characterization. Each assembly are thoroughly characterized to identify the main parameter that favours their assembly: cooperativity, thermodynamic contributions, or level of compaction. IV. Programming assembly. Numerical simulations of a trimeric assembly reveal the programming potential of stabilizing or destabilizing the assembly. More stable assemblies produce system assembling at lower concentration with narrow dynamic ranges while less stable assemblies produce system assembling at higher concentration with extended dynamic ranges. See the Supporting Information for the details regarding the simulation.

Here, we used synthetic DNA assemblies to explore the thermodynamic basis of trimeric assemblies and strategies to efficiently evolve their function (Figure 1-I, *right*). Our simple model system was designed by fusing modular DNA interacting domains with a set of different linkers (e.g., poly-T, PEG, different lengths, etc.) to promote their complexation (Figure 1-II). We then employed double-mutant cycle (DMC) analysis to determine how connectivity between the interacting domains affects their assembly mechanism through either allosteric cooperativity or configurational cooperativity (also known as the chelate effect) (Figure 1-III).[6,18] Using unfolding experiments, we also determined the origin of the thermodynamic contribution of the linkers (i.e., entropic and/or enthalpic) to the cooperativity of assembly. In agreement with our mathematical simulations, our results demonstrate that fine-tuning the chemical linkers between the interacting domains is an efficient approach to program the cooperativity of multimeric nanosystems (Figure 1-IV).

Results and Discussion

DNA-based model

To understand the design and thermodynamic principles to create cooperative molecular assembly from fusing interacting domains we designed a simple three-component assembly using the high programmability and versatility of DNA-DNA interactions.[19] As our model system, we have selected a trimeric three-way junction made of 6 binding domains fused in pair using unstructured linkers. We have designed these interacting domains to be complementary and selective for one another with similar A–T/G–C content, thereby ensuring similar stability for all interacting domains. More specifically, all our interacting domains contain 10 nucleobases (5 AT/5 GC) connected by an unstructured polythymidine or PEG linker.

Simulations reveal a link between stability and cooperativity of assembly

To demonstrate the potential of this strategy and its programmability, we first performed various numerical simulations, which explored the impact of varying the trimeric energy. The trimeric energies were varied from −20 to −25 kcal mol^{-1}, while keeping constant the binding energy of the dimeric binding interfaces (−7 kcal mol^{-1}). These simulations revealed two important trends regarding the midpoint of the transition ($[A]_{50\%}$), and the dynamic range of assembly (DR, or sensitivity), the concentration window over which the assembly occupancy shifts from 10 % to 90 %. First, the most stable assembly (ΔG_{Ass} = −25 kcal mol^{-1}, Figure 1-IV, *blue curve*) is triggered at lower component concentrations ($[A]_{50\%}$ = 15 nM) and displayed the narrowest dynamic range (DR = 9). In contrast, destabilizing this assembly by only 5 kcal mol^{-1} (ΔG_{Ass} = −20 kcal mol^{-1}, *red curve*) shifted the assembly at a 40-fold higher component concentration ($[A]_{50\%}$ = 592 nM) while extending its dynamic range by up to 81-fold (DR = 729). These results suggest that varying the trimeric assembly stability can provide an easy path to optimize the cooperativity level of a molecular assembly and thus to evolve its function.

Programming the stability and cooperativity of assemblies through linker optimization

We hypothesized that varying the linker length, or its composition, should specifically impact the trimeric energy given that the association between two binding domains (dimer) should, in principle, remain independent of the linker (Figure S1). To confirm that varying the connection between binding domains can provide a way to program the cooperativity of assembly, we created a library of various three-way junctions containing different linker lengths (Figure 2a). Using thermal denaturation, we first measured the stability of the assembly (ΔG_{Ass}) of our trimeric assemblies (Figure 2b). For example, while a 2T linker provided the most stable trimeric assembly (ΔG_{Ass} = −23.5 ± 0.2 kcal·mol^{-1}), shorter and longer linkers led to less stable assemblies ($\Delta G_{Ass,0T}$ = −20.0 ± 0.5 kcal·mol^{-1} and $\Delta G_{Ass,8T}$ = −22.2 ± 0.3 kcal·mol^{-1}). As predicted by the simulation, we found a direct correlation between the stabilities (ΔG_{Ass}), the $[A]_{50\%}$ and the dynamic ranges (DR) of the assemblies. For example, the most stable 2T linkers displayed the smallest $[A]_{50\%}$ (24 ± 1 nM) and the narrowest dynamic range (34 ± 5) (Figure 2c). In contrast, the least stable 0T shifted the assembly at a 14-fold higher component concentration ($[A]_{50\%}$ = 336 ± 57 nM) while extending its dynamic range by up to 10-fold (DR = 358 ± 75). Of note, this 0T system also displays a self-inhibited "none-all-none" mechanism, where the percentage of assembled trimers increases up to 60 % when [A] equals 1000 nM and then decreases as [A] is further increased. This self-inhibition is due to the small difference in energy between the dimeric intermediates and the trimeric assembly, thus resulting in the 0T system favoring the formation of dimers AB and AC at high excess of strand A ([A]≫[B] & [C] = 30 nM).[3d] Overall, these results suggest that programming the stability of assemblies through linker variation provides an easy path to tune their assembly dynamic range as well as creating more complex assembly profiles displaying self-inhibition mechanisms.

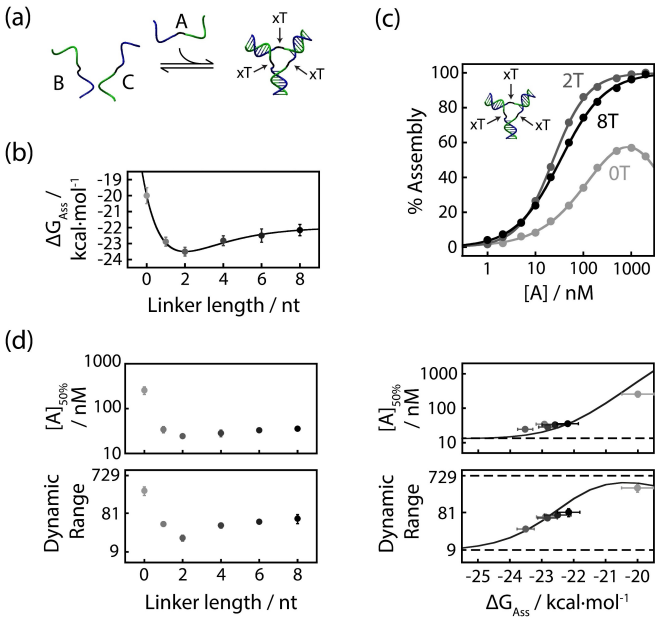

Figure 2. Programming the stability and cooperativity of molecular assemblies through linker optimization. (a) The stability of assembly of our model trimeric system, ΔG_{Ass}, can be tuned by varying the linker length (xT: the number of thymidines) connecting two 10 nucleotides interacting domains. (b) Maximal stability is achieved with a linker length of two thymidines ($\Delta G_{Ass,2T}$ = −23.5 ± 0.2 kcal·mol^{-1}). Shorter (0T) and longer (8T) linkers provide lest stable assembly ($\Delta G_{Ass,0T}$ = −20.0 ± 0.5 kcal·mol^{-1} and $\Delta G_{Ass,8T}$ = −22.2 ± 0.3 kcal·mol^{-1}). (c) The stability of the assembly impacts the assembly profile of our different trimeric nanosystems. (d) For example, the $[A]_{50\%}$, the midpoint of the assembly transition, and the dynamic range (DR), the concentration window over which the assembly occupancy shift from 10 % to 90 %, follow the same dependence to linker length than ΔG_{Ass} (left) and correlate well with our numerical simulations (right). Assemblies were performed in triplicate using 30 nM of strand B and C with increasing concentration of A in PBS buffer (50 mM Na_2HPO_4, 100 mM NaCl, pH = 7.00) at 37 °C. See Figure S2 for raw data leading to ΔG_{Ass} and Figure S3 for raw binding curves data.

Assessing the nature of cooperativity in molecular assembly

The cooperativity of assembly can be tuned through a change in assembly energy provided by variation of the linkers attaching two binding domains. Two mechanisms are typically involved to help rationalizing stabilizing effects in molecular assemblies: allostery or configurational cooperativity (Figure 3a).[6,18] In the allostery mechanism, the binding of a domain to its interacting partner is altered by the binding of an additional interacting domain (Figure 3a, *left*). This energetic connection between both interacting domains

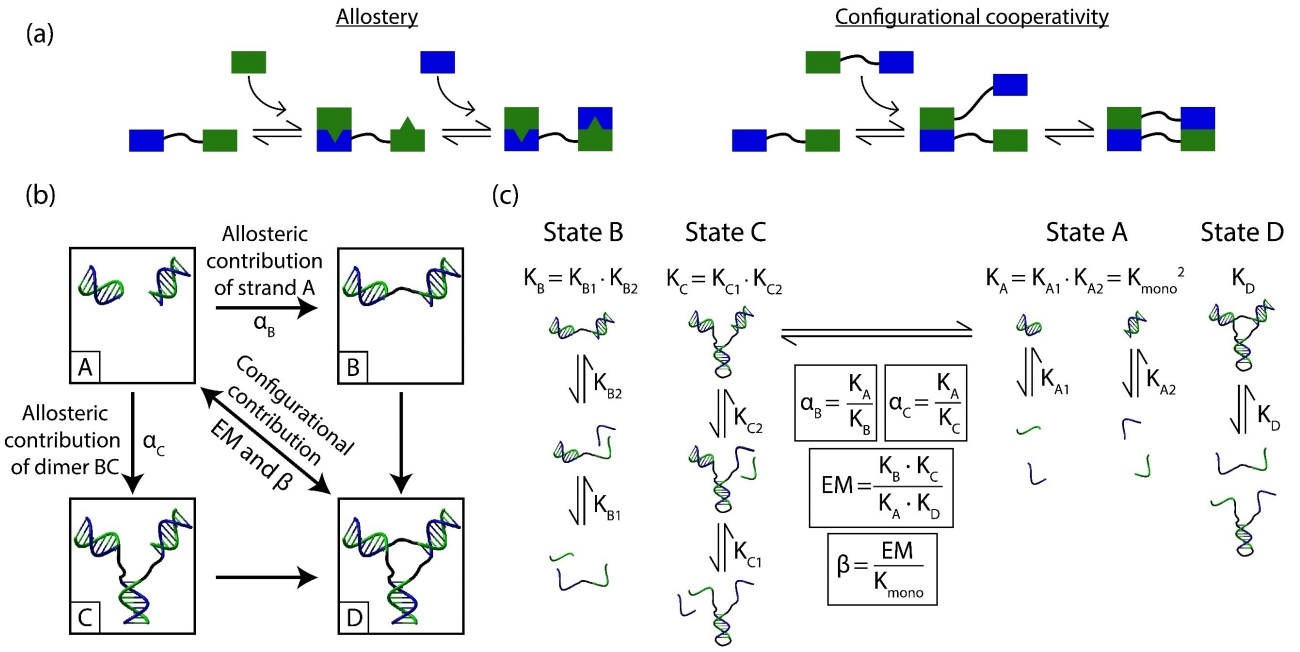

Figure 3. Assessing the contributions of allostery and configurational cooperativity using a double mutant cycle analysis. (a) In allostery, the first binding event induces a change in the state of the receptor that improves the affinity for the second binding event. In configurational cooperativity, the first binding event improves the affinity of the second binding event through an increase in effective molarity. (b) We designed a double-mutant cycle (DMC) to assess the contribution of each mechanism. The cycle starts by first measuring the intrinsic affinity of both interacting domains (state A). Then, we introduced the linkers on strand A (state B) and strand BC (state C) to address the allosteric contribution of the linker after subsequent binding of both domains (α_B and α_C, respectively). Finally, we added all linkers to the system (state D) to address the impact of bringing one interacting domain near another through an increase in effective molarity (EM). (c) The allosteric cooperativity (α_B and α_C) and the configurational cooperativity (β) can be estimated by measuring all the experimentally accessible equilibrium constants of each state (K_A, K_B, K_C and K_D). All equilibrium constants presented here are defined as dissociation constants. Notably, for the K_C and K_D equilibrium, strands B (green) and C (blue) were covalently linked together using a 4T loop to ensure that they remained in a dimeric state and did not disassemble during the analysis.

is typically considered to occur through a conformational change, but it can also be mediated through changes in dynamic properties.[6] The binding of oxygen to haemoglobin, for instance, represents a well-known example of allostery where the binding of the first oxygen molecule to haemoglobin increases the affinity of the three other binding sites through a global dynamic conformational change.[20] In the configurational cooperativity mechanism, the binding of a domain to its binding partner is enhanced by an increase in effective molarity caused by its attachment to a second interacting domain nearby (Figure 3a, *right*). Such cooperative binding is often exploited in drug design where, for example, two drugs are chemically linked together to increase the strength of interaction with a protein receptor containing two close binding sites.[21]

Distinguishing allostery from configurational cooperativity with double-mutant cycles

To explore the relative contributions of allostery and configurational cooperativity to the assembly of our model systems, we performed a double-mutant cycle (DMC) analysis.[18b] This type of cycle is often used to dissect the specific energetic contribution of a mutation, a motif or a structure from all the interactions typically present in a system.[16,18b, 22] Here, we simplified the DMC analysis of our DNA assemblies to the binding on the last strand (i.e., binding of strand A to the dimer BC) given that all DNA interacting domains are energetically equivalent and that the overall stability of the assembly (ΔG_{Ass}) is directly proportional to this last assembly step (Figure S1). DMC analysis (Figure 3b) began with assessing the intrinsic affinity of each individual interacting domain between strand A and its respective binding partners in the preformed dimer BC (state A). We then introduced the linker on strand A (state B) and on the preformed dimer BC (state C) to address the allosteric contributions of these linkers to the subsequent binding of both interacting domains (α_B and α_C, respectively). Finally, we introduced both linkers into the system (state D) to address the impact of bringing one interacting domain near another through configurational cooperativity (β). For all these cooperative parameters (α_B, α_C and β), a value higher than unity indicates a positive cooperative effect, while values lower than unity indicate a negative cooperative effect.

All thermodynamic parameters of the cycle can be directly measured by determining the dissociation constants involved in each state of the cycle (see equations in Figure 3c). We started the cycle by measuring the intrinsic

binding affinity between the individual interacting domains without the presence of the linkers, K_{mono}, i.e., the 10 bp duplex containing 5 AT and 5 GC (state A). As expected, we found that the two interacting domains involved in the closing of the DNA assembly display similar affinities of 8.5 ± 0.8 nM (K_{D1}) and 9.2 ± 0.5 nM (K_{D2}) (Figure 4a, State A), thus providing an average K_{mono} of 8.8 ± 0.7 nM.

Allosteric contributions are negligeable. We then characterized the allosteric contribution of linking the two interacting domains of strand A to the successive binding of its respective binding partners on strand B (K_{B1}) and strand C (K_{B2}) (Figure 4b, State B). For example, we found that the first binding event (K_{B1}) of the 2T system displayed a higher binding constant of 96 ± 2 nM compared to K_{mono}, corresponding to a destabilization of 1.5 ± 0.1 kcal·mol^{-1}. Increased destabilization was also observed when employing longer linkers with K_{B1} varying from 77 ± 4 nM (0T) to 139 ± 6 nM (8T). This increase in K_{B1} is likely attributable to additional charge repulsion and steric hindrance created by the presence of additional nucleotides in the vicinity of the interacting domain. In contrast, the second binding event (K_{B2}) of the 2T system displayed a binding constant similar to K_{mono} (4.3 ± 0.3 nM), suggesting that the double helix minimizes charge repulsion and/or improves the accessibility of the second interacting domain. Interestingly, all linkers displayed a binding constant of approximately 4.1 ± 0.3 nM (1T to 8T), except for the 0T system, which showed a much lower binding constant of 0.7 ± 0.1 nM. This is likely attributable to potential base-stacking interactions between the nucleotides at the extremities of both duplexes.[23] Overall, these stabilizing or destabilizing effects are not large enough to significantly impact the stability of the assembly. Indeed, the allosteric contribution quantified by α_B remains slightly below unity ($0.1 < \alpha_B < 3$) for all assemblies (Figure 4b, left). From these α_B values, we calculated that the allosteric contribution of the linker on strand A destabilizes the assembly of the three-way junction by 0.93 ± 0.05 kcal·mol^{-1} (1T) to 1.22 ± 0.02 kcal·mol^{-1} (8T), while the absence of a linker (0T) has a negligible contribution of -0.2 ± 0.1 kcal·mol^{-1}.

We then characterized the allosteric contributions of the linkers on the preformed dimer BC to the successive binding of its two respective binding partners (K_{C1} and K_{C2}) on strand A (Figure 4c, State C). For example, we found that the first binding event (K_{C1}) of the 2T system displayed a higher binding constant of 58 ± 13 nM than K_{mono}, corresponding to a destabilization of 1.2 ± 0.2 kcal·mol^{-1} for the hybridization of the first DNA binding domain. Similarly, all systems containing thymidine linkers (1T to 8T) displayed binding constants higher than K_{mono} starting from 98 ± 6 nM (1T) and plateauing at approximately 33 ± 8 nM (8T). This decrease in K_{C1} may be attributable to the increased distance between the interacting domain and the bulky negatively charged stem loop of the preformed dimer. In contrast, the absence of linkers (0T) resulted in a more stable system with a binding constant of 28 ± 4 nM ($K_{C1,0T}$), which suggests potential base stacking between the two duplexes.[23] In contrast, the second binding event (K_{C2}), which takes place near two double helices, displayed binding constants similar to K_{mono} for linkers ranging from 2T to 8T (7.8 ± 0.4 nM). Interestingly, the shorter linkers (0T and 1T) behaved in the opposite manner to their first binding events. While the first binding event of the 0T system displayed a higher affinity than its second binding event ($K_{C1,0T} < K_{C2,0T}$), the opposite trend was observed for the 1T system ($K_{C2,1T} < K_{C1,1T}$). This discrepancy, however, cancels out and provides allosteric factors displaying small negative contributions ($0.1 < \alpha_C < 1$), with α_C remaining below unity with an upwards trend when the length of the linker was increased (Figure 4c, *middle*). The allosteric impact of linking the blue and green domains together, therefore, destabilizes the assembly of the three-way junction by 1.24 ± 0.09 kcal·mol^{-1} (0T) to 0.7 ± 0.2 kcal·mol^{-1} (8T). Overall, we found that both allosteric factors (α_B and α_C) remain too small to rationalize the large impact of the linker length on the stability of the assembly. This suggests that the addition of these linkers did not induce a change in conformation significant enough to affect their binding affinities. Indeed, the two allosteric contributions (α_B and α_C) contribute less than 5 % of the stability of the assembly (Table S1–S2).

Configurational cooperativity is the key contributor. Given that the allosteric contributions of the linkers were found to be relatively small, we determined the contribution of configurational cooperativity coming from bringing two interacting domains into such close proximity. To do so, we determined the effective molarity (EM) of all systems by measuring the affinity of strand A towards the preformed dimer BC containing its respective binding partners (K_D) using thermal denaturation (Figure 4a, State D). We found that K_D showed a bell-shaped distribution, with the 2T system being the most stable (1.8 ± 0.2 pM) by two orders of magnitude compared to the less stable 8T system (170 ± 85 pM). This translates into an effective molarity of 0.3 ± 0.1 mM for the 2T system compared to 5 ± 1 μM for the 8T system. We then calculated the contributions of the configurational cooperativity (β) and found that it follows a similar trend to ΔG_{Ass} (Figure 2b), varying between $(5 \pm 2) \times 10^2$ (8T) and $(4 \pm 2) \times 10^4$ (2T) (Figure 4c, *right*). In contrast to the allosteric contributions, which have negligible effects on the assembly ($0.1 < \alpha_B, \alpha_C < 3$), the configurational cooperativity contribution β was found to be 2 to 5 orders of magnitude larger ($500 < \beta < 40\,000$). This represents, for example, a configurational cooperativity contribution of 7.4 ± 0.2 kcal·mol^{-1} for the 2T system and 4.4 ± 0.2 kcal·mol^{-1} for the 8T system (Table S1–S2). Overall, these results indicate that configurational cooperativity is the major determinant in stabilizing our DNA-based assemblies.

The most stable and cooperative linkers optimize enthalpy

Having identified configurational cooperativity as the main determinant of cooperative assembly of our DNA-based model, we then explored whether this effect arises more from an enthalpic or an entropic contribution. To do so, we performed thermal denaturation of our assemblies and determined their ΔH_{Ass} and ΔS_{Ass} (Figure 5a). We found that the variation in enthalpy of our systems correlated well with

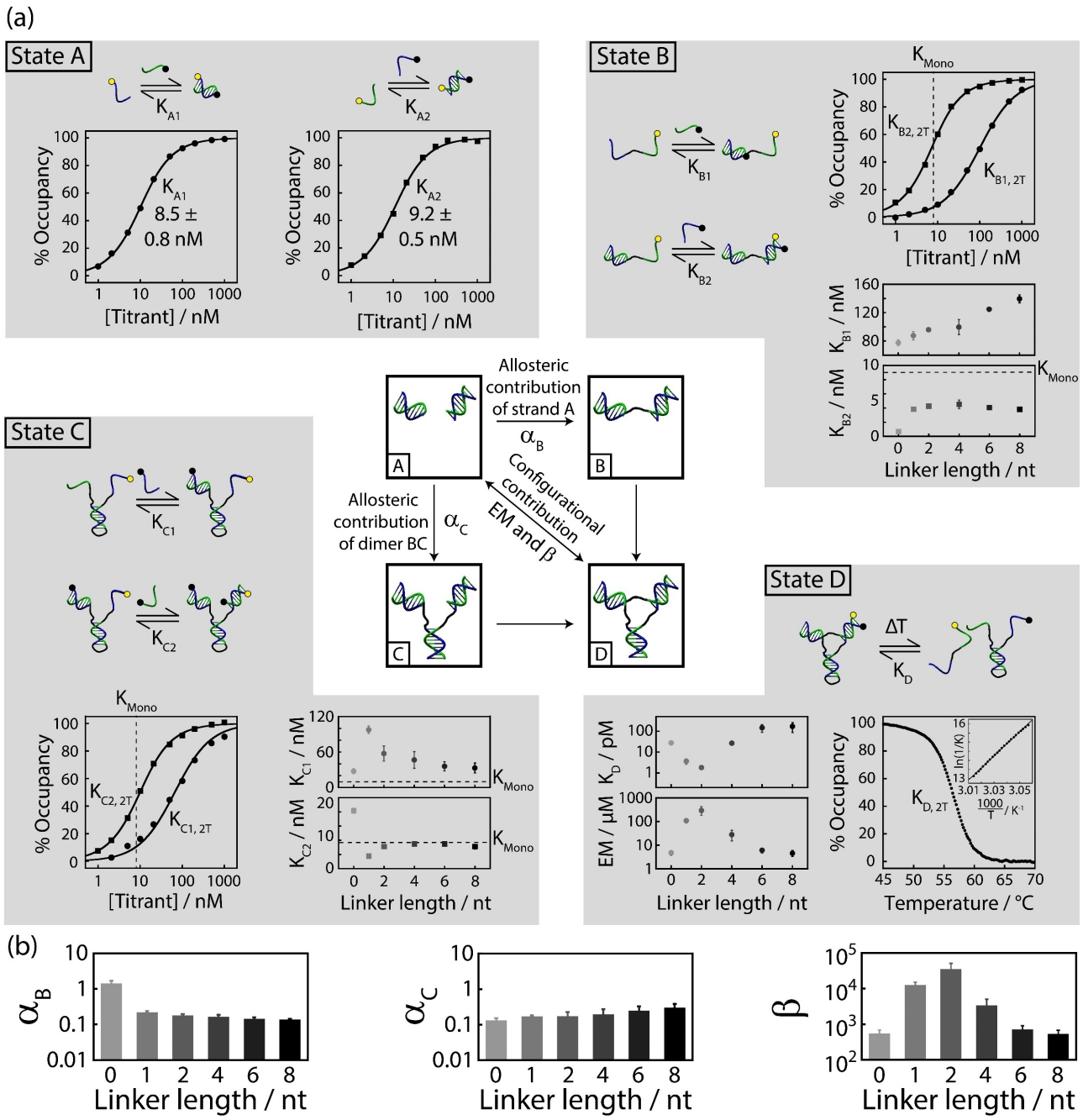

Figure 4. Configurational cooperativity (β) is the main determinant of the difference in assembly stability (ΔG_{Ass}) observed among all molecular assemblies built with various linker lengths. (a) State A. Characterization of the intrinsic affinity of the two interacting domains without linkers (K_{A1} and K_{A2}). State B. Characterization of the allosteric contribution of linking together two interacting domains of strand A on the successive binding of its respective binding partners on strand B (K_{B1}) and strand C (K_{B2}). State C. Characterization of the allosteric contribution of the linkers on the preformed dimer BC to the successive binding of its two respective binding partners (K_{C1} and K_{C2}) on strand A. State D. Characterization of the configurational cooperativity contribution of both linkers on the final assembly measured by thermal denaturation (K_D). (b) The DMC analysis reveals that the allosteric contribution of linking two interacting domains remains mainly negligible ($0.1 < \alpha_B < 3$ and $0.1 < \alpha_C < 1$). Configurational cooperativity (β), in contrast, remains the main determinant of the stability improvement of the assembly ($10^2 < \beta < 10^5$), with a contribution up to 5 orders of magnitude higher than the allosteric contributions. Refer to Figure 3 for the calculation of each parameter (α_B, α_C, EM and β). For clarity, only the binding curves and the melting curves of the 2T system are shown; see Figure S4 (K_{A1}-K_{A2}), Figure S5 (K_{B1}-K_{B2}), Figure S6 (K_{C1}-K_{C2}) and Figure S7 (K_D) for the full dataset. Each binding constant corresponds to the average and standard deviation of three independent binding curves (see Table S1 for values). All DNA strands are chemically labelled with either a fluorophore moiety (FAM, yellow circle) or a quencher moiety (BHQ-1, black circle). All equilibrium constants are reported as dissociation constants. Experiments were performed at 37 °C in PBS (50 mM Na_2HPO_4, 100 mM NaCl, pH = 7.00).

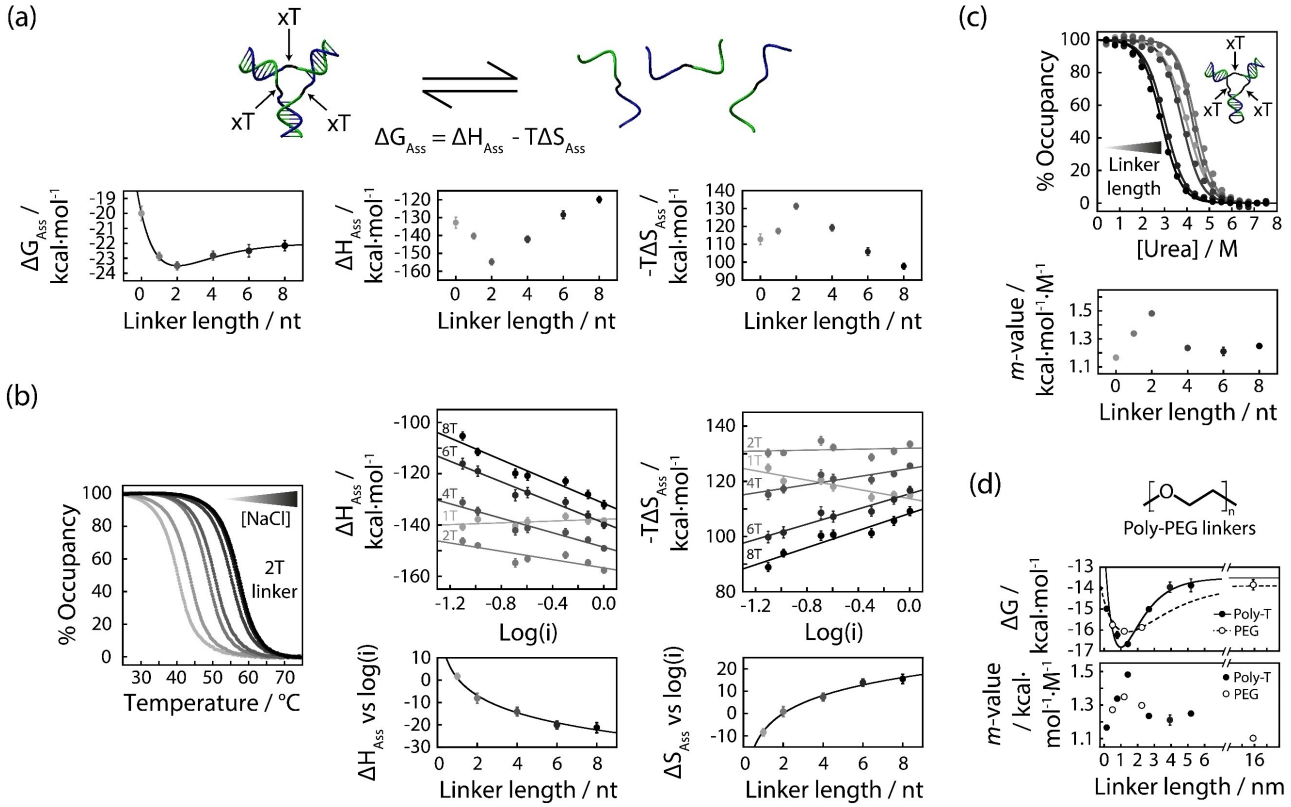

Figure 5. High stability arises from the increase in enthalpy and level of compaction. (a) ΔH_{Ass} and ΔS_{Ass} measured through thermal denaturation (Figure S2) showed that the contribution of the linkers is not purely entropic when the length of the linker is increased. (b) To facilitate assembly, we increased the ionic strength to overcome the electrostatic repulsion between the negatively charged polythymidine linkers and the interacting domains (Figure S10). For longer linkers (>2T), we found that higher ionic strength led to stronger enthalpic contributions and less favourable entropic contributions. In contrast, we found that both the enthalpic and entropic contributions of the 1T system decreased with increasing ionic strength, suggesting that this assembly displays fewer interactions and becomes less ordered at high salt concentrations. Interestingly, the ΔH_{Ass} and the ΔS_{Ass} of the individual interacting domains remain relatively unchanged with increasing ionic strength (Figure S9, Table S3), suggesting that the variation observed in the trimeric assemblies is likely attributable to the structural variation taking place upon the formation of the three-way junction. (c) Urea denaturation (Figure S11) showed that the higher stability of the 2T system comes from its ability to bury more surfaces upon assembly, i.e., a larger *m*-value. (d) A less bulky linker, such as PEG (Figure S12), also led to trends and observations similar to those of the polythymidine linkers. See Tables S3–S6 for all values. All thermal denaturation experiments were performed in PBS with varying NaCl concentrations, and all urea denaturation experiments were performed at 37 °C in PBS (50 mM Na_2HPO_4, 100 mM NaCl, pH = 7.00).

the variation in free energy, with the 2T linker system displaying both the strongest ΔH_{Ass} (-155 ± 2 kcal·mol^{-1}) and ΔG_{Ass} (-23.5 ± 0.3 kcal·mol^{-1}). In contrast, the entropic contribution displayed an opposite correlation with ΔG_{Ass}. For example, the assembly of the most stable 2T system was found to be the most entropically unfavourable (131 ± 2 kcal·mol^{-1}). Since the interacting domains remain constant among our different assemblies, these enthalpic and entropic variations likely originate from the different linkers and their impact on the conformation of the junction. As observed in other systems, we also observed enthalpy-entropy compensation among our different assemblies (Figure S8).[24] This suggests that the enthalpically favourable interactions arising from varying linker length also produce an unfavourable entropic contribution, likely via mobility restriction.

We decided to further explore the nature of the enthalpic contribution. Since the linkers are negatively charged and increasing their length may lead to further charge repulsion, we hypothesized that increasing the ionic strength may improve stability by minimizing charge repulsion. Using thermal denaturation, we measured the ΔH_{Ass} and the ΔS_{Ass} of all our systems (1T to 8T) at various sodium chloride concentrations (Figure 5b). We first measured the impact of ionic strength on the interacting domains in the absence of the linker and found that their ΔH and ΔS of assembly remained relatively unchanged (Figure S9). This implies that any variations measured on the trimeric assemblies are likely attributable to the structural variations taking place upon the formation of the three-way junction. We thus determined the ΔH and ΔS of our trimeric assemblies and found that increasing the ionic strength of the solvent generally increased both ΔH_{Ass} and ΔS_{Ass} (Figure 5b). As expected, increasing the ionic strength resulted in a higher ΔH_{Ass}, likely by reducing charge repulsion between the linkers and the DNA binding domains. The observed increase in ΔS_{Ass} with ionic strength, on the other hand, suggests that the three-way junction becomes more

ordered as charge repulsion decreases. Interestingly, however, we noted that despite having the most favourable ΔH_{Ass}, the optimal 2T system displays only a small decrease in ΔH_{Ass} with increasing ionic strength and almost no variation in ΔS_{Ass}. This result suggests that the 2T junction probably remains similarly ordered at various ionic strengths, perhaps due to an already optimal compaction of its junction. In comparison, junctions made with longer linkers displayed increased ΔS_{Ass} with increasing ionic strength, suggesting that the assembly becomes more ordered at high salt concentrations. In contrast, we found that both the enthalpic and entropic contributions of the 1T decreased with increasing ionic strength, suggesting that this assembly displays fewer interactions and becomes less ordered at high salt concentrations. Given that the linker length for the 1T system is too short for optimal stability, one hypothesis explaining this behaviour may be that increasing the salt concentration stabilizes the formation of an optimal "2T-like" junction leading to the dissociation of one base pair in the interacting domains (9 bp vs. 10 bp). Overall, these results demonstrate that the 2T linker optimizes the stability of the trimeric assembly by maximizing its ΔH_{Ass}.

High stability and cooperativity of assembly correlates with high level of compaction

We wanted to further explore the physical determinants behind the strong enthalpic contribution of the 2T assembly. For this purpose, we performed urea denaturation experiments to measure the variation in accessible surface area (ΔASA) or level of compaction of each assembly (Figure 5c).[25] This was done by determining the *m*-value of each unfolding transition, a parameter that measures how ΔG varies with the urea concentration, which correlates with the accessible surface area. Surprisingly, we found that the 2T system buries 17 % more surface area during its assembly (*m*-value $= 1.481 \pm 0.009$ kcal·mol^{-1}·M^{-1}, Figure 5c, *left*) than the 4T, 6T and 8T systems (average *m*-value $= 1.23 \pm 0.02$ kcal·mol^{-1}·M^{-1}).[26] This suggests that the 2T linker stabilizes a more compact assembly that maximizes solvent exclusion upon assembly.[27] In contrast, assemblies with longer linkers (>2T) displayed lower *m*-values, suggesting that their junctions are more exposed to solvent molecules. This result is also consistent with the ionic strength experiments: water-filled junctions (4T, 6T, 8T) were more sensitive to salt concentrations (Figure 5b). In contrast, we observed that the 0T and 1T assemblies displayed lower *m*-values, with the 0T system displaying the least compact conformation. This is likely due to the possibility that these assemblies are not able to form the same number of interactions as the 2T system due to steric hindrance between the interacting domains at the branchpoint.[28] Overall, these results provide strong evidence that the extra enthalpic contribution at the origin of the high cooperativity of the 2T assembly is due to additional interactions at the junction providing optimal packing between the interacting domains.

Similar conclusions were also reached by employing PEG linkers instead of polythymidine linkers to link the interacting domains. The same thermal and urea denaturation experiments (Figure S12) revealed that the stability of the PEG linker systems followed the same bell-shaped behaviour as the polythymidine linker systems, with the optimal PEG system being slightly less stable (-16.1 ± 0.1 kcal·mol^{-1}) than its thymidine counterpart (-16.8 ± 0.2 kcal·mol^{-1}) (Figure 5d). Similarly, we found that the stability of all PEG systems correlated well with their level of compaction (Table S5–S6). Interestingly, we also found that the PEG linker system requires a slightly longer linker for optimal stability (1.34 ± 0.03 nm) compared to its polythymidine counterpart (1.00 ± 0.07 nm). The improved stability provided by polythymidine linkers compared to PEG linkers may be rationalized by stronger intermolecular interactions between the thymidine linkers (e.g., H-bonding, and base stacking). In combination, these results suggest that the linker properties (length or nature) are important determinants in creating compact junctions in molecular assemblies. This also suggests that the cooperativity level of molecular assemblies could be easily tuned or evolved through simple optimization of the length of a linker connecting two interacting domains (e.g., insertion/deletion mutations).

Optimizing assembly profiles through linker design

We confirmed that tuning the linker length and therefore the level of compaction of our model trimeric assembly provide a relatively simple and straightforward strategy to program the cooperativity of molecular assemblies by stabilizing or destabilizing the assembly (Figure 6). For example, we have demonstrated the relationships between the stability (ΔG_{Ass}), the $[A]_{50\%}$ and the dynamic range as suggested by the strong overlapping of the experimental and simulated data (Figure 2). In these experiments, however, all the linkers were changed simultaneously, which did not provide a predictable way to tune the stability of the assembly (i.e., the stability was found maximal for an intermediate length of 2T). We thus hypothesized that varying only one linker while keeping the other constant may enhanced our ability to precisely control both the $[A]_{50\%}$ and the dynamic range via slight variations in the level of compaction of the assembly (Figure 6a). For example, we found that increasing the length of only one linker enabled precise and linear programming of ΔG_{Ass}, which also correlated well with the level of compaction and the assembly parameters ($[A]_{50\%}$ and DR) (Figure 6a). Of note the optimal stability and level of compaction was reached using an asymmetrical trimer that contains two 2T linkers and one 0T linker.

The link between ΔG_{Ass}, $[A]_{50\%}$ and the dynamic range was further confirmed by varying the temperature (i.e., lower temperature stabilizes the assembly while higher temperature destabilizes it). Using the 2T (Figure 6b) and 8T (Figure 6c) linker assemblies, we also confirmed that an increase in 10 °C provided a programming ability ($[A]_{50\%}$

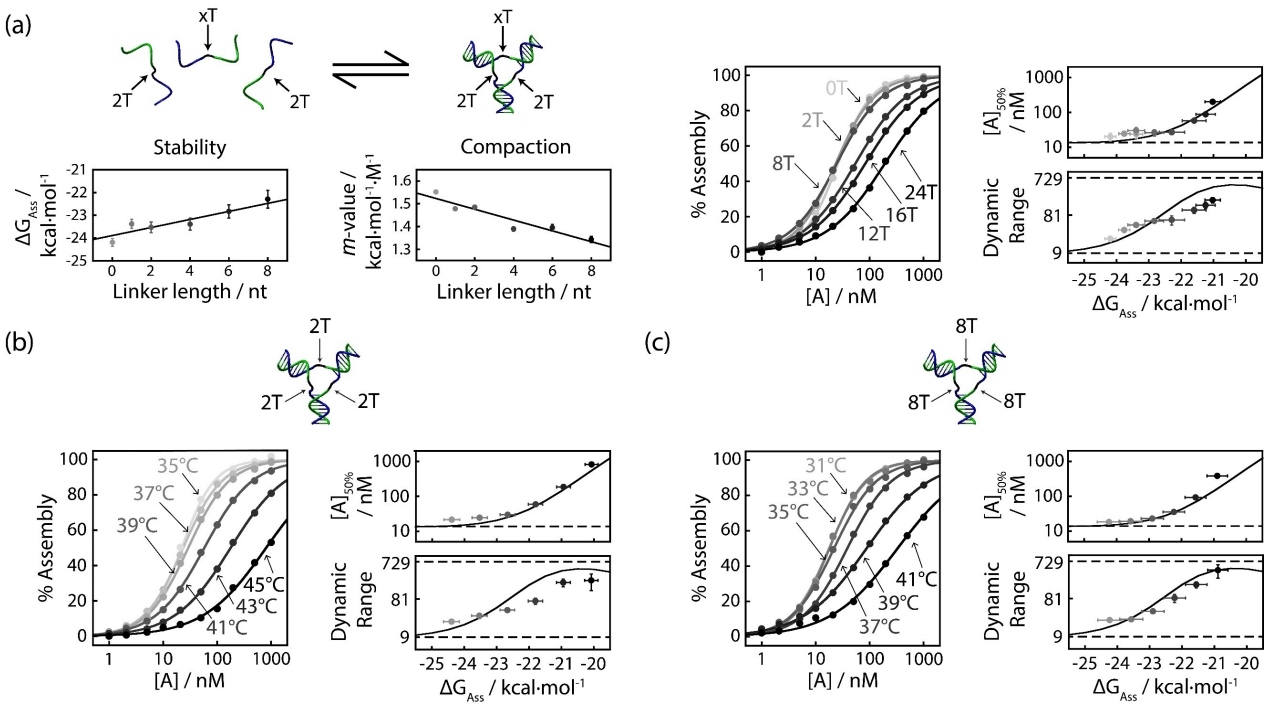

Figure 6. Programming the assembly profile of trimeric assemblies by tuning stability via various linker lengths. (a) A more precise way to program the level of compaction, and thus the stability of the assembly consists of changing only one linker while keeping the two others at the optimal length of 2T (see Figure S13 and Figure S14). The assembly properties ($[A]_{50\%}$ and DR) correlate well with the stability of the assembly (ΔG_{Ass}) and our mathematical simulation (black line). (c-d) The stability of the assemblies (here, the 2T and 8T systems) can also be programmed by tuning the temperature, thus also enabling precise programming of the assembly properties. All binding experiments were performed in triplicate in PBS (50 mM Na_2HPO_4, 100 mM NaCl, pH = 7.00) at 37 °C if not mentioned otherwise. For all raw binding curves, see Figure S15 (panel a), Figure S16 (panel b) and Figure S17 (panel c).

and DR) similar to that of linker variation (nearly two orders of magnitude). These results exemplify the simplicity with which the assembly profile of molecular assemblies can be optimized and evolved by simply shortening (deletion mutation) or increasing (insertion mutation) the linkers between their interacting domains, thereby adjusting the level of compaction of the assembly and thus its stability. This ability to program the cooperativity and the stability of molecular assemblies can also be useful in synthetic biology or system chemistry to develop self-sorting nanosystems that distinguish between components solely based on their respective stabilities.[29]

Conclusion

Here, we have demonstrated how cooperative molecular assemblies can be readily created by fusing interacting domains, and their assembly profile precisely programmed by tuning their level of compaction through linker optimization between the interacting domains. We have demonstrated this by exploiting the high programmability and versatility of DNA-DNA interactions to create a simple trimeric "three-way junction" model system. As expected, we have first shown that the optimal cooperativity of assembly can be reached through an intermediate linker length that offers optimal stability (not too short, not too long). Using a double-mutant cycle analysis, we determined that the effect provided by the optimal linker (2T) was mainly attributable to high configurational cooperativity ($\beta > 1000$) despite displaying negative allosteric contributions ($0.1 < \alpha_B$, $\alpha_C < 3$) (Figure 3 and 4). By further exploring the thermodynamic basis of these assemblies, we were, however, surprised to discover that the high cooperativity was mainly attributable to a maximization of the enthalpic contribution rather than a minimization of the entropic contribution as this has been suggested in other previous studies.[9] Indeed, we found that the 2T system produces the largest enthalpic contribution due to its ability to bury larger interacting surfaces at the interface of all components (Figure 5). This suggests that the optimal linker helps to form favorable intermolecular interactions at the centre of the junction, therefore removing water molecules while forming a more compact assembly. Finally, we showed that simple variation in the linker length between two interacting domains in a trimeric assembly also enables easy programming of its assembly profile ($[A]_{50\%}$ and DR) (Figure 6).

Engineering molecular assemblies by connecting interacting domains through various linker length and composition provides a simple and programmable chemical strategy to optimize the assembly cooperativity of any self-assembled nanosystem. Here, we have demonstrated this concept using a DNA-based model system through simple variation of the length of an unstructured polythymidine linker. The univer-

sality of this design concept was further validated by replacing the polythymidine linker with a more flexible, less bulky PEG linker. Furthermore, all assembly profiles with different dynamic ranges and $[A]_{50\%}$ were also well modelled mathematically as a simple function of their stability, demonstrating the programmable and quantitative nature of this strategy. We believe that the ability to program the stability and cooperativity of the assembly of small self-assembled building blocks may also find applications to simplify the assembly of larger nanostructures. DNA three-way junctions, for example, are a simple building block for the assembly of the larger DNA tetrahedron, a common DNA nanostructure used in biosensing and drug delivery.[30] These are typically assembled through a long and time-consuming annealing protocol favoring the most thermodynamically stable structure. But such protocol also typically prevents the incorporation of temperature-sensitive components.[31] We have also shown that the efficient assembly of a trimeric nanostructure requires a large difference in energy between the dimeric intermediates and the trimeric assembly. For example, the yield of assembly of our 0T three-way junction (Figure 2c) was only about 60 % and could not be improved by increasing the concentration of one of its components. The controlled self-assembly of small building blocks, or "developmental" self-assembly, has become a promising avenue and has recently been reported for the isothermal assembly of larger DNA nanostructures.[32] This strategy is also reminiscent of "self-sorting" in system chemistry,[29] and the self-assembly of protein components in cell, which happens sequentially and isothermally in a crowded environment.[17d] We thus believe that a better thermodynamic control on the smaller building blocks could help researchers to better design self-assembled nanosystems with precise control and sophisticated functions.

Although we have employed nucleic acids and PEG molecules as a model system to demonstrate the thermodynamic rules to program the assembly of cooperative (or not) nanosystems, our conclusion may also apply to other chemical systems. Indeed, scientists have shown that fusing protein interacting domains using intrinsically disordered linkers can create a variety of molecular assemblies with different stabilities.[7b,33] For example, by changing the length of a flexible peptide linker between two DHFR proteins, researchers have observed different levels of oligomerization.[17a] Varying the linker length in fused proteins[34] or fused ligands[35] was also shown to improve affinity through the avidity effect. More specifically, PROTAC drugs could benefit from linker optimization that maximizes compaction and cooperative PPI interactions to promote the assembly of the ternary complex, thus preventing self-inhibition and the Hook effect.[36] This linker optimization strategy could also be applied for the design of supramolecular systems to obtain optimized assembly characteristics, which better mimic the functional diversity and complexity of biological multimeric systems.[3d,17d] Furthermore, since ΔG_{Ass} is intrinsically related to the cooperativity of assembly (Figure 6), we anticipate that recent progress in computational design may assist the discovery of the linker that provide the optimal dynamic range.[37]

The ability to narrow or broaden the dynamic range of molecular functions remains important both for living organisms and for the development of various biotechnologies. One well-known alternative strategy to program the dynamic range of functional nanosystems consists of creating allosteric systems.[14,38] One limitation of allosteric strategies, however, remains its design complexity, since it typically requires the creation of energetically interconnected binding sites into single- or multidomain nanosystems.[39] In contrast, we have shown here that multiple interacting domains can readily form in a cooperatively self-assembled nanosystem through a simple optimization of the linkers connecting the interacting domains. This strategy seems to have occurred extensively during evolution to create functional protein complexes through, for example, gene fusion events where the genes coding for two interaction domains are fused into one open reading frame.[40] During evolution, these fused complexes can often acquire long interdomain linkers that can play a key role in their function.[41] In summary, we believe that our findings can provide chemists and biochemists with a simple thermodynamic framework to create self-assembled nanosystems with programmable assemblies while improving our understanding of mechanisms that may have driven the evolution of multidomain protein complexes.

Acknowledgements

This research was conducted through the Natural Sciences and Engineering Research Council of Canada (NSERC) Discovery Grants (RGPIN-2020-06975) (A.V.-B). A.V.-B. is Canada Research Chair in Bioengineering and Bionanotechnology, Tier II. D. L. acknowledge a scholarship from the Fonds de recherche du Québec – Nature et technologies (FRQNT) 3rd cycle (#256330 and #290101). The authors would like to thank J. Pelletier and M. Merkx for the helpful comments on the paper.

Conflict of Interest

There are no conflicts to declare.

Data Availability Statement

The data that support the findings of this study are available from the corresponding author upon reasonable request.

Keywords: Cooperativity · DNA Nanotechnology · Protein Complexes · Self-Assembly · Supramolecular Chemistry

[1] M. Lynch, *Mol. Biol. Evol.* **2012**, *29*, 1353–1366.
[2] a) E. Mattia, S. Otto, *Nat. Nanotechnol.* **2015**, *10*, 111–119; b) N. C. Seeman, H. F. Sleiman, *Nat. Rev. Mater.* **2017**, *3*,

17068; c) D. M. Raymond, B. L. Nilsson, *Chem. Soc. Rev.* **2018**, *47*, 3659–3720.
[3] a) N. J. Marianayagam, M. Sunde, J. M. Matthews, *Trends Biochem. Sci.* **2004**, *29*, 618–625; b) K. Hagner, S. Setayeshgar, M. Lynch, *Phys. Rev. E* **2018**, *98*, 062401; c) C. Bou-Nader, J. Zhang, *Molecules* **2020**, *25*, 2881; d) D. Lauzon, A. Vallée-Bélisle, *Nat. Chem.* **2023**, *15*, 458–467.
[4] M. H. Ali, B. Imperiali, *Bioorg. Med. Chem.* **2005**, *13*, 5013–5020.
[5] M. D. W. Griffin, R. C. J. Dobson, F. G. Pearce, L. Antonio, A. E. Whitten, C. K. Liew, J. P. Mackay, J. Trewhella, G. B. Jameson, M. A. Perugini, J. A. Gerrard, *J. Mol. Biol.* **2008**, *380*, 691–703.
[6] A. Whitty, *Nat. Chem. Biol.* **2008**, *4*, 435–439.
[7] a) J. E. Dueber, E. A. Mirsky, W. A. Lim, *Nat. Biotechnol.* **2007**, *25*, 660–662; b) X. Chen, J. L. Zaro, W.-C. Shen, *Adv. Drug Delivery Rev.* **2013**, *65*, 1357–1369; c) Y. Bai, Q. Luo, J. Liu, *Chem. Soc. Rev.* **2016**, *45*, 2756–2767.
[8] Y. Wang, A. G. Cheetham, G. Angacian, H. Su, L. Xie, H. Cui, *Adv. Drug Delivery Rev.* **2017**, *110–111*, 112–126.
[9] a) D. Mariottini, A. Idili, M. A. D. Nijenhuis, G. Ercolani, F. Ricci, *J. Am. Chem. Soc.* **2019**, *141*, 11367–11371; b) D. Mariottini, A. Idili, M. A. D. Nijenhuis, T. F. A. de Greef, F. Ricci, *J. Am. Chem. Soc.* **2018**, *140*, 14725–14734.
[10] a) M. Y. X. Ma, K. McCallum, S. C. Climie, R. Kuperman, W. C. Lin, M. Sumner-Smith, R. W. Barnett, *Nucleic Acids Res.* **1993**, *21*, 2585–2589; b) J. Zhou, P. Swiderski, H. Li, J. Zhang, C. P. Neff, R. Akkina, J. J. Rossi, *Nucleic Acids Res.* **2009**, *37*, 3094–3109.
[11] a) G. W. Gokel, W. M. Leevy, M. E. Weber, *Chem. Rev.* **2004**, *104*, 2723–2750; b) J. Wu, K. C.-F. Leung, D. Benítez, J.-Y. Han, S. J. Cantrill, L. Fang, J. F. Stoddart, *Angew. Chem. Int. Ed.* **2008**, *47*, 7470–7474.
[12] R. Kumar, A. Sharma, H. Singh, P. Suating, H. S. Kim, K. Sunwoo, I. Shim, B. C. Gibb, J. S. Kim, *Chem. Rev.* **2019**, *119*, 9657–9721.
[13] S. Rinaldi, *Molecules* **2020**, *25*, 3276.
[14] F. Ricci, A. Vallée-Bélisle, A. J. Simon, A. Porchetta, K. W. Plaxco, *Acc. Chem. Res.* **2016**, *49*, 1884–1892.
[15] S. B. Shuker, P. J. Hajduk, R. P. Meadows, S. W. Fesik, *Science* **1996**, *274*, 1531–1534.
[16] L. K. S. von Krbek, A. J. Achazi, M. Solleder, M. Weber, B. Paulus, C. A. Schalley, *Chem. Eur. J.* **2016**, *22*, 15475–15484.
[17] a) J. C. T. Carlson, S. S. Jena, M. Flenniken, T.-f. Chou, R. A. Siegel, C. R. Wagner, *J. Am. Chem. Soc.* **2006**, *128*, 7630–7638; b) W. A. Lim, *Nat. Rev. Mol. Cell Biol.* **2010**, *11*, 393–403; c) R. van der Lee, M. Buljan, B. Lang, R. J. Weatheritt, G. W. Daughdrill, A. K. Dunker, M. Fuxreiter, J. Gough, J. Gsponer, D. T. Jones, P. M. Kim, R. W. Kriwacki, C. J. Oldfield, R. V. Pappu, P. Tompa, V. N. Uversky, P. E. Wright, M. M. Babu, *Chem. Rev.* **2014**, *114*, 6589–6631; d) Y. Tu, F. Peng, A. Adawy, Y. Men, L. K. E. A. Abdelmohsen, D. A. Wilson, *Chem. Rev.* **2016**, *116*, 2023–2078.
[18] a) J. R. Williamson, *Nat. Chem. Biol.* **2008**, *4*, 458–465; b) L. K. S. von Krbek, C. A. Schalley, P. Thordarson, *Chem. Soc. Rev.* **2017**, *46*, 2622–2637.
[19] a) Y. Tang, B. Ge, D. Sen, H.-Z. Yu, *Chem. Soc. Rev.* **2014**, *43*, 518–529; b) S. G. Harroun, C. Prévost-Tremblay, D. Lauzon, A. Desrosiers, X. Wang, L. Pedro, A. Vallée-Bélisle, *Nanoscale* **2018**, *10*, 4607–4641; c) F. Wang, X. Liu, I. Willner, *Angew. Chem. Int. Ed.* **2015**, *54*, 1098–1129.
[20] Y. Yuan, M. F. Tam, V. Simplaceanu, C. Ho, *Chem. Rev.* **2015**, *115*, 1702–1724.
[21] P. S. Portoghese, *Trends Pharmacol. Sci.* **1989**, *10*, 230–235.
[22] S. L. Cockroft, C. A. Hunter, *Chem. Soc. Rev.* **2007**, *36*, 172–188.
[23] S. H. Ha, J. E. Ferrell, *Science* **2016**, *352*, 990–993.
[24] a) J. D. Chodera, D. L. Mobley, *Annu. Rev. Biophys.* **2013**, *42*, 121–142; b) X. Du, Y. Li, Y.-L. Xia, S.-M. Ai, J. Liang, P. Sang, X.-L. Ji, S.-Q. Liu, *Int. J. Mol. Sci.* **2016**, *17*, 144.
[25] A. Idili, F. Ricci, A. Vallée-Bélisle, *Nucleic Acids Res.* **2017**, *45*, 7571–7580.
[26] a) J. K. Myers, C. N. Pace, J. M. Scholtz, *Protein Sci.* **1995**, *4*, 2138–2148; b) V. M. Shelton, T. R. Sosnick, T. Pan, *Biochemistry* **1999**, *38*, 16831–16839.
[27] a) S. Muhuri, K. Mimura, D. Miyoshi, N. Sugimoto, *J. Am. Chem. Soc.* **2009**, *131*, 9268–9280; b) S.-i. Nakano, D. Miyoshi, N. Sugimoto, *Chem. Rev.* **2014**, *114*, 2733–2758.
[28] T. Sabir, A. Toulmin, L. Ma, A. C. Jones, P. McGlynn, G. F. Schröder, S. W. Magennis, *J. Am. Chem. Soc.* **2012**, *134*, 6280–6285.
[29] a) M. M. Safont-Sempere, G. Fernández, F. Würthner, *Chem. Rev.* **2011**, *111*, 5784–5814; b) D. Serrano-Molina, C. Montoro-García, M. J. Mayoral, A. de Juan, D. González-Rodríguez, *J. Am. Chem. Soc.* **2022**, *144*, 5450–5460.
[30] N. Xie, S. Liu, X. Yang, X. He, J. Huang, K. Wang, *Analyst* **2017**, *142*, 3322–3332.
[31] R. Jungmann, T. Liedl, T. L. Sobey, W. Shih, F. C. Simmel, *J. Am. Chem. Soc.* **2008**, *130*, 10062–10063.
[32] a) P. Yin, H. M. T. Choi, C. R. Calvert, N. A. Pierce, *Nature* **2008**, *451*, 318–322; b) J. P. Sadowski, C. R. Calvert, D. Y. Zhang, N. A. Pierce, P. Yin, *ACS Nano* **2014**, *8*, 3251–3259; c) A. T. Glynn, S. R. Davidson, L. Qian, *J. Am. Chem. Soc.* **2022**, *144*, 10075–10079.
[33] a) J. S. Klein, S. Jiang, R. P. Galimidi, J. R. Keeffe, P. J. Bjorkman, *Protein Eng. Des. Sel.* **2014**, *27*, 325–330; b) M. van Rosmalen, M. Krom, M. Merkx, *Biochemistry* **2017**, *56*, 6565–6574; c) C. S. Sørensen, M. Kjaergaard, *Proc. Natl. Acad. Sci. USA* **2019**, *116*, 23124–23131.
[34] C. S. Sørensen, A. Jendroszek, M. Kjaergaard, *J. Mol. Biol.* **2019**, *431*, 4784–4795.
[35] E. T. Mack, P. W. Snyder, R. Perez-Castillejos, B. Bilgiçer, D. T. Moustakas, M. J. Butte, G. M. Whitesides, *J. Am. Chem. Soc.* **2012**, *134*, 333–345.
[36] C. Cecchini, S. Pannilunghi, S. Tardy, L. Scapozza, *Front. Chem.* **2021**, *9*, 672267.
[37] a) T. J. Magliery, *Curr. Opin. Struct. Biol.* **2015**, *33*, 161–168; b) J. N. Zadeh, C. D. Steenberg, J. S. Bois, B. R. Wolfe, M. B. Pierce, A. R. Khan, R. M. Dirks, N. A. Pierce, *J. Comput. Chem.* **2011**, *32*, 170–173; c) P. W. J. M. Frederix, I. Patmanidis, S. J. Marrink, *Chem. Soc. Rev.* **2018**, *47*, 3470–3489.
[38] a) F. Ricci, A. Vallée-Bélisle, A. Porchetta, K. W. Plaxco, *J. Am. Chem. Soc.* **2012**, *134*, 15177–15180; b) D. Lauzon, A. Vallée-Bélisle, *J. Am. Chem. Soc.* **2023**, *145*, 18846–18854.
[39] a) L. A. Churchfield, A. Medina-Morales, J. D. Brodin, A. Perez, F. A. Tezcan, *J. Am. Chem. Soc.* **2016**, *138*, 13163–13166; b) F. Pirro, N. Schmidt, J. Lincoff, Z. X. Widel, N. F. Polizzi, L. Liu, M. J. Therien, M. Grabe, M. Chino, A. Lombardi, W. F. DeGrado, *Proc. Natl. Acad. Sci. USA* **2020**, *117*, 33246–33253.
[40] a) Å. K. Björklund, D. Ekman, S. Light, J. Frey-Skött, A. Elofsson, *J. Mol. Biol.* **2005**, *353*, 911–923; b) J. A. Marsh, S. A. Teichmann, *Annu. Rev. Biochem.* **2015**, *84*, 551–575.
[41] a) M. Bashton, C. Chothia, *J. Mol. Biol.* **2002**, *315*, 927–939; b) T. Perica, Joseph A. Marsh, Filipa L. Sousa, E. Natan, Lucy J. Colwell, Sebastian E. Ahnert, Sarah A. Teichmann, *Biochem. Soc. Trans.* **2012**, *40*, 475–491; c) Y. Wang, J. C. Fisher, R. Mathew, L. Ou, S. Otieno, J. Sublet, L. Xiao, J. Chen, M. F. Roussel, R. W. Kriwacki, *Nat. Chem. Biol.* **2011**, *7*, 214–221.

Manuscript received: September 25, 2023
Accepted manuscript online: November 17, 2023
Version of record online: November 17, 2023

Research Articles

DNA Nanotechnology

D. Lauzon, A. Vallée-Bélisle* **e202313944**

Design and Thermodynamics Principles to Program the Cooperativity of Molecular Assemblies

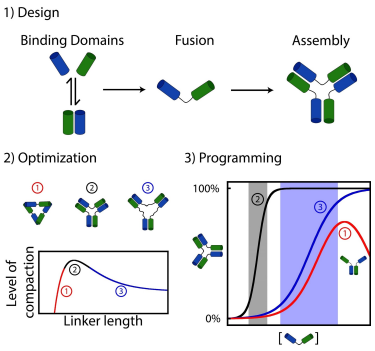

Molecular assembly can be designed by fusing binding domains. A precise optimization of the level of compaction of the assembly using linker of different lengths or compositions can provide a simple strategy to program their assembly properties (e.g., midpoint, dynamic range, and inhibition). The thermodynamic and mechanistic principles demonstrated herein also shine light behind the evolution of biological molecular assembly.